A Letters Journal Exploring the Frontiers of Physics

October 2022

EPL, **140** (2022) 11004
doi: 10.1209/0295-5075/ac954b

www.epljournal.org

# Dissipative cooling towards phantom Bethe states in boundary-driven XXZ spin chain

Vladislav Popkov[1,2(a)] and Mario Salerno[3]

[1] *Faculty of Mathematics and Physics, University of Ljubljana - Jadranska 19, SI-1000 Ljubljana, Slovenia*
[2] *Bergisches Universität Wuppertal - Gauss Str. 20, D-42097 Wuppertal, Germany*
[3] *Dipartimento di Fisica "E.R. Caianiello", and INFN, Gruppo Collegato di Salerno, Università di Salerno Via Giovanni Paolo II, I-84084 Fisciano (SA), Italy*

received 24 July 2022; accepted in final form 27 September 2022
published online 10 October 2022

**Abstract** – A dissipative method that allows to access the family of phantom Bethe states (PBS) of boundary-driven $XXZ$ spin chains is introduced. The method consists in coupling the ends of the open spin chain to suitable dissipative magnetic baths to force the edge spins to satisfy specific boundary conditions necessary for the PBS existence. Cumulative monotonous depopulation of the non-chiral components of the density matrix with growing dissipation amplitude is analogous to the depopulation of high-energy states in response to thermal cooling. Compared to generic states, PBS have strong chirality, non-trivial topology and carry high spin currents.



**Introduction.** – Dissipation does not need to be always destructive for quantum protocols but it can represent a resource for manipulating quantum systems. Dissipation alone [1] or in combination with coherent dynamics [2–10], indeed, can be used to create quantum non-equilibrium stationary states (NESS) which are attractors of the dynamics and therefore are stable even in the presence of noise.

Most protocols, however, require a tailored set of operations used in pumping cycles to target each specific state [5,11]. If the protocols are implemented by stationary control fields, they usually require sophisticated dissipations that make the NESS targeting more complicated [12].This is due to the fact that the targeted NESS must be an eigenstate of the coherent part of the dynamics and a dark state for all jump operators in the dissipator [13,14].

Here we demonstrate how to generate a remarkable family of NESS containing an arbitrary number of qubits, employing simple boundary-localized dissipation, and manipulating just one parameter. These are the phantom Bethe states (PBS), *i.e.*, eigenstates of integrable $XXZ$ spin chains on special parameter manifolds [15–17], possessing unusual chiral and topological features.

The phenomenon is based on a subtle mechanism that makes (within the quantum Zeno limit [18–21]), a highly selective "phantom" invariant subspace the basin of attraction for the density matrix. Consequently, the NESS responds in a singular resonant way to an increase of the dissipation strength in the vicinity of "phantom" manifolds, restricting the density matrix to states with chirality of the same sign and thus rendering the NESS chiral. The resonances become sharper as the dissipation strength is increased and their number grows with the number of spins involved.

Dynamically, the "freezing out" of the non-chiral components of the density matrix with growing dissipation amplitude is analogous to the depopulation of high-energy states in response to thermal cooling.

The "dissipative cooling" method consists in coupling the ends of the open chain to dissipative baths of polarization constraining the first and the last spin to relax to predefined pure qubit states that satisfy boundary conditions necessary for the PBS existence. We show that by changing the control parameter, *i.e.*, the misfit azimuthal angle of the dissipatively targeted boundary polarizations,

(a) E-mail: vladipopkov@gmail.com (corresponding author)

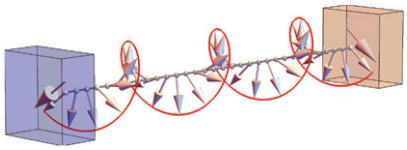

Fig. 1: Model setup. An open $XXZ$ spin chain is edge-coupled to dissipative fully polarizing baths (blue and pink boxes). When baths' polarizations (big arrows inside boxes) match eq. (8), phantom Bethe states carrying large spin currents come into existence. The figure shows a pure spin-helix state corresponding to case $M_+ = 0$ in eq. (8).

it is possible to thread "phantom" manifolds, passing from one chiral NESS to another one with different topology (see fig. 2). To the best of our knowledge, a quantum protocol that allows to target the whole PBS family is presently lacking.

The simplest states belonging to the phantom family are the spin-helix states (SHS) (see top panel of fig. 4 for an example). Recently, SHS were created and used as a sensitive tool to measure the anisotropy in experiments on $XXZ$ chains implemented via ultracold atoms [22,23]. While in [22,23] the lifetime of the SHS is restricted by finite size effects, the stability of dissipatively created SHS (and other PBS) is guaranteed as long as the boundary dissipation strength is kept sufficiently strong.

Note that while SHS are pure states, all other PBS are mixed states corresponding, in terms of the mean variation of the magnetization along the chain, to helices with a variable radius (see middle panel of fig. 4 for an example). Quite interestingly, we find that in comparison to generic pure and mixed states of the open $XXZ$ chain, the PBS have strong chirality and carry relatively high spin currents (see fig. 3), a feature that can be of potential interest for future applications.

**Model setting and near Zeno limit relaxation.** – Our dissipative setup is schematically depicted in fig. 1. An $XXZ$ Heisenberg spin $\frac{1}{2}$ chain of $N+2$ sites, numbered as $0, 1, \dots N+1$, is coupled to Lindbladian baths of polarizations at the ends [18,24], see details in the Supplementary Material `Supplementarymaterial.pdf` (SM). We assume dissipative targeting of generic pure qubit states $\rho_{L,R} = (I + \vec{n}_{L,R}\cdot\vec{\sigma})/2$ at sites 0 and $N+1$, where $\vec{n}_L$, $\vec{n}_R$ are unit vectors of polarization. The strength of the dissipation $\Gamma$ is measured by the inverse time needed for edge spins to relax, *e.g.*, $\rho_{L/R}(t) = \frac{I}{2} + \frac{1}{2}\vec{\sigma}_1\vec{n}_{L/R} + O(e^{-\Gamma t})$, if the coherent part ($XXZ$ spin chain Hamiltonian) is neglected. If $\vec{n}_L \neq \vec{n}_R$, a non-equilibrium gradient is created and a spin current $j^z$ can flow, typically obeying the Fourier law $j^z = O(1/N)$.

In (8) we fix a resonance condition under which steady currents can be increased up to maximally possible values, $j^z = O(1)$. Using the criterion of [25] one finds that the NESS is always unique.

It was shown in [26] that close to quantum Zeno limit $\Gamma \to \infty$ the relaxation to NESS undergoes a three-stage process, each stage occurring at different timescale. On the shortest timescale: $t \leq O(1/\Gamma)$, the boundary spins relax towards their targeted states. From this point on, the density matrix is approximately given by $\rho = \rho_L \otimes R(t) \otimes \rho_R$, where $R(t) = \mathrm{tr}_{L,R}\rho(t)$ describes the time evolution of the the internal part of the system, which becomes approximately coherent again [2] and is governed by the dissipation projected Hamiltonian $h_D$ given by [26]

$$h_D = \sum_{n=1}^{N-1} \vec{\sigma}_n \cdot \hat{J}\vec{\sigma}_{n+1} + \hat{J}\vec{n}_L\cdot\vec{\sigma}_1 + \hat{J}\vec{n}_R\cdot\vec{\sigma}_N, \qquad (1)$$

with $\hat{J} = \mathrm{diag}(1,1,\Delta)$. Note that the dissipation-projected Hamiltonian (1) depends on polarizations of the baths through its boundary fields.

On the intermediate timescale: $O(1/\Gamma) \ll t \leq O(1)$, the reduced density matrix $R(t)$ acquires the approximate form

$$R(t) = \sum_\alpha P_\alpha(\tau) \mid \alpha\rangle\langle\alpha \mid + O\left(\frac{1}{\Gamma}\right), \qquad (2)$$

where $\tau = \frac{t}{\Gamma}$ and $|\alpha\rangle$ are $h_D$ eigenstates, with positive coefficients $P_\alpha$ significantly changing on long time scales $\tau = O(1)$. Finally, on the long time scale $O(1) \ll t \leq O(\Gamma)$ the coefficients $P_\alpha(\tau) \to P_\alpha(\infty) \equiv P_\alpha$ relax to their stationary NESS values, by following the effective Markov process

$$\frac{\partial P_\alpha(\tau)}{\partial\tau} = \sum_{\beta\neq\alpha} w_{\beta\alpha}P_\beta(\tau) - \sum_{\beta\neq\alpha} w_{\alpha\beta}P_\alpha(\tau) \qquad (3)$$

with rates $w_{\alpha\beta} \equiv w_{\alpha\to\beta}$ given by [26]

$$w_{\alpha\beta} = |\langle\beta \mid g_L \mid \alpha\rangle|^2 + |\langle\beta \mid g_R \mid \alpha\rangle|^2, \qquad (4)$$

where $g_L, g_R$ are operators acting on the first and the last spin respectively, given by

$$g_L = g(\vec{n}_L)\otimes I^{\otimes_{N-1}}, \quad g_R = I^{\otimes_{N-1}}\otimes g(\vec{n}_R), \qquad (5)$$

$$g\left(\vec{n}(\theta,\varphi)\right) = \hat{J}\left(\vec{n}\left(\frac{\pi}{2}-\theta,\varphi+\pi\right) - i\vec{n}\left(\frac{\pi}{2},\varphi+\frac{\pi}{2}\right)\right)\cdot\vec{\sigma}, \qquad (6)$$

where $\theta, \varphi$ are spherical coordinates of a unit vector. The final state, the NESS, in the Zeno limit has the form

$$\rho_{NESS}^{Zeno} = \rho_L \otimes \left(\sum_\alpha P_\alpha \mid \alpha\rangle\langle\alpha \mid\right) \otimes \rho_R, \qquad (7)$$

where $P_\alpha$ is the time-independent solution of (3), and $\mid\alpha\rangle$ are eigenstates of $h_D$ (1).

**Phantom Bethe states.** – Phantom Bethe states are eigenstates of the Hamiltonian (1) that have exceptional chirality and correspond to special manifolds of the boundary fields in (1) $\hat{J}\vec{n}_L(\theta_L,\varphi_L)$, $\hat{J}\vec{n}_R(\theta_R,\varphi_R)$, with $\theta, \varphi$ given by [15,16]

$$\theta_L = \theta_R, \quad \varphi_R - \varphi_L = (N+1-2M_+)\gamma, \qquad (8)$$

where $M_+ = 0, 1, \dots N+1$ (see footnote [1]) and $\gamma$ parametrizing the $XXZ$ model anisotropy $\Delta$

$$\Delta = \cos\gamma. \tag{9}$$

The substitution $M_+ \to M_- \equiv N+1-M_+$ in (8) leads to the physical setup with the opposite boundary gradient, $\varphi_R - \varphi_L \to -(\varphi_R - \varphi_L)$, and consequently flips the steady current $j^z \to -j^z$. The respective NESSs are related via the left-right reflection $\varphi_L \leftrightarrow \varphi_R$ and subsequent rotation in the $XY$ plane, see the SM. Using this property we restrict the $M_+$ range to the $M_+ = 0, 1, \dots, [\frac{N+1}{2}]$.

For fixed $M \equiv M_+$ in this range all eigenstates $|\,\alpha\rangle$ of $h_D$ (1) which determine Zeno NESS (7) split into two chiral families, $\{|\,\alpha_+\rangle\}$, $\{|\,\alpha_-\rangle\}$ characterized by the so-called phantom Bethe roots [15]. All eigenstates from each family share common chiral properties [16]. Introducing the function $b(n,m) = \sum_{k=n}^{m} \binom{N}{k}$, the number of eigenstates $d_+, d_-$ in $\{|\,\alpha_+\rangle\}$, $\{|\,\alpha_-\rangle\}$ is given by $d_\pm = b(0, M_\pm)$. In addition, in our case (8) a smaller invariant subfamily $\{|\,\alpha_+^{(1)}\rangle\} \in \{|\,\alpha_+\rangle\}$ exists (see the SM), yielding further splitting $\{|\,\alpha_+\rangle\} = \{|\,\alpha_+^{(1)}\rangle\} \oplus \{|\,\alpha_+^{(2)}\rangle\}$ where $d_+^{(1)} = b(M-1, M) = \binom{N+1}{M}$, $d_+^{(2)} = b(0, M-2)$.

According to the above, the reduced density matrix $R$ in (2) on "phantom" manifolds (8) splits as

$$R \approx \sum_{\kappa=1}^{2} \sum_{\alpha_+^{(\kappa)}=1}^{d_+^{(\kappa)}} P_{\alpha+}^{(\kappa)}(\tau)\; |\,\alpha_+^{(k)}\rangle\langle\alpha_+^{(k)}\,| + \sum_{\alpha_-=1}^{d_-} P_{\alpha-}(\tau)\; |\,\alpha_-\rangle\langle\alpha_-\,|\,. \tag{10}$$

The sum (10) contains projectors on states with opposite chiralities and is generically approximately neutral. The time evolution obeys the effective Markov process (3), *i.e.*, depends on rates $w_{\beta\delta}$ exclusively. Analyzing the rates (see the SM) we find a remarkable property: all the rates

$$w_{\alpha_+^{(1)} \to \alpha_-} = w_{\alpha_+^{(1)} \to \alpha_+^{(2)}} = 0 \tag{11}$$

vanish, while generic $w_{\beta \to \alpha_+^{(1)}}$ remain finite. Thus, the subfamily $\{|\,\alpha_+^{(1)}\rangle\}$ becomes an adsorbing basin of the Markov process (3) [27] resulting in depopulation of all other states with time, and leading to the NESS of the form

$$\rho_{NESS}^{Phantom}(M) = \rho_L \otimes \left( \sum_{\alpha_+^{(1)}=1}^{\binom{N+1}{M}} P_{\alpha_+^{(1)}}\; |\,\alpha_+^{(1)}\rangle\langle\alpha_+^{(1)}\,| \right) \otimes \rho_R. \tag{12}$$

[1] Phantom Bethe roots criterium for open $XXZ$ spin chain with boundary fields is given by eq. (17) of [16]. For our special case $h_D$ (1) we set $\alpha_+ = \alpha_- = -\eta = -i\gamma$, $\beta_+ + \beta_- = 0$, $\theta_- = i(\pi - \varphi_L)$, $\theta_+ = i(\pi - \varphi_R)$, $1/\cosh(\beta_-) = \sin\theta_L$, $\tanh(\beta_-) = -\cos\theta_L$, leading to eq. (8), with $M = 0, \dots, N-1$. Another choice of parameters $\alpha_+ = \alpha_- = \eta = i\gamma$, $\beta_+ + \beta_- = 0$, $\theta_- = -i\varphi_L$, $\theta_+ = -i\varphi_R$, $1/\cosh(\beta_-) = \sin\theta_L$, $\tanh(\beta_-) = \cos\theta_L$ leads to the same $h_D$. Inserting it into eq. (17) of [16] leads to the same eq. (8) with $M \to M+2$, thus enlarging the $M$ range in (8) to values $M = 0, \dots, N+1$.

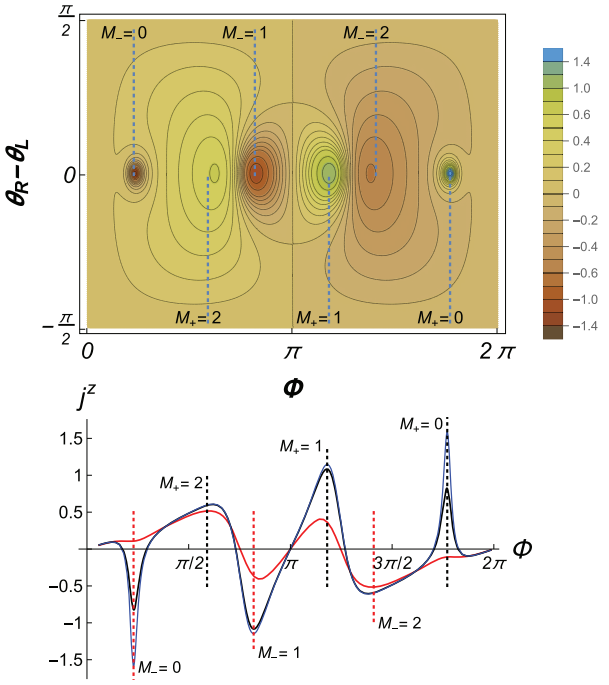


Fig. 2: Top panel: steady magnetization current $j^z$ *vs.* boundary misfits of azimuthal angle $\Phi = \varphi_R - \varphi_L$ and polar angle $\theta_R - \theta_L$, in Zeno limit, for $N = 5, \Delta = 0.6, \theta_L = \pi/2$, and $\varphi_L = 0$. The targeted spin polarizations are $\vec{n}_L = (1,0,0), \vec{n}_R = (\sin\theta_R\cos\Phi, \sin\theta_R\sin\Phi, \cos\theta_R)$. Bottom panel: cut of the $j^z$ surface at $\theta_R - \theta_L = 0$, for different dissipation strengths $\Gamma = 20, 100, 1000$ (more spiky functions correspond to increasing $\Gamma$. Vertical black and red dotted lines indicate the misfit angles $\Phi = \pm(N+1-2M)\gamma$.

All eigenstates $|\,\alpha_+^{(1)}\rangle$ in (12) are phantom Bethe eigenstates [15] of the same chirality and the chirality gets more pronounced for small $M$. For $M = 0$, the sum in (12) contains just one term, a projector on the spin-helix state (SHS) (13),

$$\Psi_{SHS}(\gamma) = \bigotimes_{k=1}^{N} \begin{pmatrix} \cos\frac{\theta_L}{2} \\ \sin\frac{\theta_L}{2}\; e^{ik\gamma + i\varphi_L} \end{pmatrix}, \tag{13}$$

visualized in fig. 1, characterized by a large current of magnetization

$$j_{SHS} = \langle 2(\sigma_n^x\sigma_{n+1}^y - \sigma_n^y\sigma_{n+1}^x)\rangle_{SHS} = 2\sin^2\theta_L\;\sin\gamma. \tag{14}$$

A possibility to target spin-helix state (13) dissipatively was also noted in previous studies [14,28,29].

For $M > 0$ the ideal helix (13) gets blurred but the NESS (12) remains chiral. For $M = 1$ the current of magnetization $\langle\alpha_+\,|\hat{j}^z|\,\alpha_+\rangle$ averaged over states $|\,\alpha_+\rangle$ is of the order $\langle j^z(M)\rangle \approx j_{SHS}(1-2/N)$, while for arbitrary $M < N/2$, estimates yield $\langle j^z(M)\rangle \approx j_{SHS}(1-2M/N)$ [16].

From the above result we predict the existence of chiral Zeno NESS with unusually high magnetization current at phantom Bethe manifolds (8).

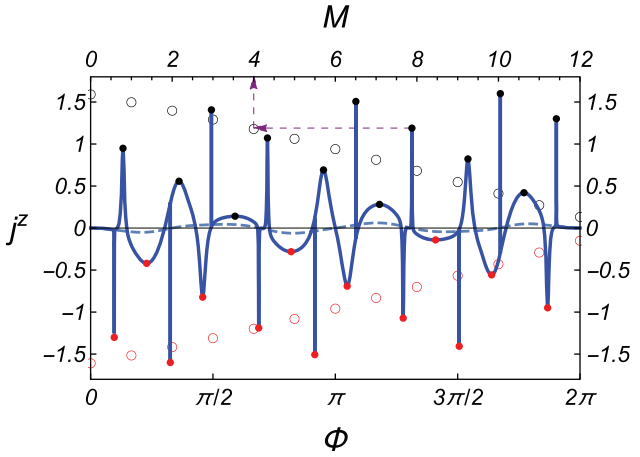


Fig. 3: Steady magnetization current $j^z$ (blue curve) *vs.* $XY$ plane misfit angle $\Phi = \varphi_R - \varphi_L$ (bottom horizontal axis) in the Zeno limit $\Gamma \to \infty$, computed using the method in [31,32]. Parameters are: $N = 25$, $\Delta = 0.6, \theta = \pi/2$. $\Phi$ coordinates of black/red dots correspond to angles $\Phi_c(M) = \varphi_R - \varphi_L$ with $M = 0, 1, \ldots, N+1$ in (7). The dashed blue line shows $j_z$ *vs.* $\Phi$ for a chain with an additional boundary misfit $\pi/6$ in the polar angle: $\vec{n}_L = (1, 0, 0)$, $\vec{n}_R = (\frac{\sqrt{3}}{2}\cos\Phi, \frac{\sqrt{3}}{2}\sin\Phi, \frac{1}{2})$. The empty black and red circles referring to the top horizontal axis permit to identify the values of $M$ associated to each $j^z$ peak, as indicated by the purple dashed lines with arrows (find the corresponding open circle of equal amplitude and read the $M$ value on the top horizontal axis).

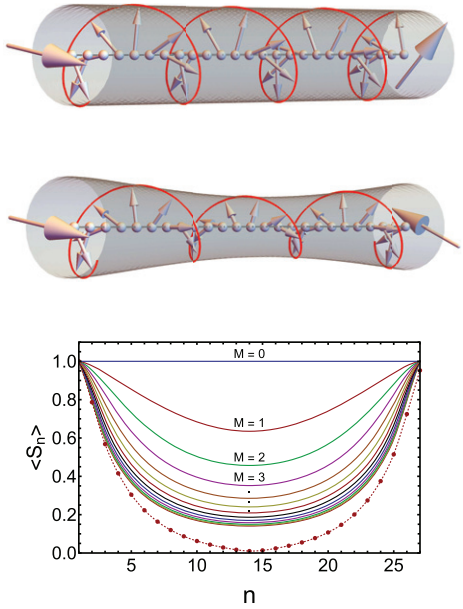


Fig. 4: Top and middle panels: PBS of the $XXZ$ open chain with $N = 25$ and for cases $M = 0$ (top panel) and $M = 1$ (middle panel) in eq. (8). The $z$-axis is directed along the chain while the left big arrow points in the positive $x$-direction. Bottom panel: variation of the averaged spin (helix radius) along the chain for $M = 0, 1, ..., 12$ (curves from top to bottom, respectively). The dotted curve at the bottom, depicted for comparison, refers to a generic NESS out of the phantom manifold. All parameters are fixed as in fig. 3.

**Numerical results.** – To check our predictions we study NESS magnetization current for fixed anisotropy $\Delta$ and varying boundary gradient, for systems of size $4 \le N \le 30$. We use exact numerical diagonalization for small chains [30] and Matrix product ansatz for NESS in the Zeno limit [31,32] for large chains. Already for $N = 5$ we find all $j^z$ peak positions at predicted points (8) and their vicinity, see fig. 2. Namely, all points (8) with $M_\pm = 0, 1, 2$ correspond to peaks of various amplitudes ($j^z = 0$ for $M_+ = (N+1)/2 = 3$, since they correspond to zero misfit angle $\Phi = \pm(N + 1 - 2M_+)\gamma = 0$ and hence to absence of the boundary gradient $\vec{n}_L = \vec{n}_R$).

For larger chains (fig. 3) the agreement and the phenomenon becomes striking: most $j^z$ peaks appear as sharp resonances centered at phantom Bethe states manifolds (8), on top of a background with $j^z = O(1/N)$. Notice that the empty black and red circles in fig. 3 show the dependence of the $j^z$ peaks on $M$ (top horizontal axis).

The role of the parameter $M$ determining the NESS rank in (12) via $r(M) = \binom{N+1}{M}$ deserves special discussion. The highest and sharpest of all $j^z$ peaks always corresponds to $M_\pm = 0$, see figs. 2, 3, *i.e.*, to pure Zeno NESS, with the magnetization winding in a perfect helix around the $z$-axis, see (13) and fig. 4. For $M > 0$, perfect chirality is lost: the basis of "phantom" manifold for $M = 1$ consists of 2 disjointed helix pieces separated by a kink at some position $n$; phantom Bethe states are linear combinations of basis states for all possible kink positions [16]. The resulting NESS magnetization profile is a distorted helix with variable radius, see middle panel of fig. 4. Basis states for arbitrary $M$ contain $M$ kinks [16], introducing more helix imperfections. For large $M$ NESS becomes a mixture of exponentially large number of states. *E.g.*, the peak with $M = 8$ in fig. 3 has $\binom{26}{8} > 1.5{*}10^6$ contributing states, about 5% of full Hilbert space containing $2^{25}$ states. Nevertheless, due to the similar chiral properties of all contributing components, the respective NESS is chiral.

In fig. 4 we show typical PBS profiles of the $XXZ$ chain with $N = 25$, for different $M$ values. We see that for each $M$ there is a specific variation of the helix radius (curves in the bottom panel) for the corresponding PBS. Notice that as $M$ increases the PBS curves accumulate toward a limiting curve which is well above the curve corresponding to a generic NESS out of the phantom manifold (bottom line with dots). Thus, quite interestingly, the magnetization profile for all "phantom" manifolds $0 < M \le N/2$ is qualitatively different from that of typical (non-chiral) NESS. This fact also well correlates with the large $j^z$ current observed for PBS with respect to generic NESS.

It is also worth noting that, due to larger number of contributing states, peaks with larger $M$ are less sharp and

have smaller amplitude, but, on the other side, the NESS gets more stable with respect to perturbations (boundary misfits, lowering dissipation, etc.). This effect can be seen by comparing the behavior of peaks at increasing $\theta_R - \theta_L$ misfit (upper panel of fig. 2) and for different $\Gamma$ values (the bottom panel).

In particular, as $\Gamma$ decreases, the near Zeno limit description of an effectively coherent evolution (2) becomes invalid, and the peaks gradually smear out, the sharper peaks first. In contrast, for parameters chosen away from "phantom" manifolds, variations of $\Gamma$ do not lead to any drastic effects (data not shown), especially for large enough $N$. The reason is, beyond a certain characteristic value $\Gamma > \Gamma_{ch}(N) = O(1/N)$, the effective quantum Zeno regime sets in.

**Conclusion.** – We demonstrated that the spikes of the steady magnetization current in open $XXZ$ spin chains with dissipatively created boundary gradient are due to the existence of special manifolds (8) where phantom Bethe roots solutions of the Bethe Ansatz equations exist. The mechanism by which the PBS can be physically accessed was identified to be the strong dissipation which drives the system towards a chiral invariant subspace. The gradual depopulation of the non-chiral states resembles the depopulation of highly energetic states in a quantum system coupled to a cold thermal bath. The amplitude of dissipation plays the role of inverse temperature and a chiral subset of states plays the role of a subset of low-energy states close to the ground state of the system. We showed that, by varying the system size, the bulk anisotropy and the boundary dissipative driving, one can manipulate a number of peaks of the magnetization current, the distance between the peaks in the parameter space, and their magnitudes. All the resulting stationary states are easily distinguishable by the value of the carried spin current, and by their non-trivial topology [33].

We expect the dissipative cooling approach considered in this paper to be effective also for other open quantum many body systems that are integrable via the off-diagonal Bethe ansatz method.

* * *

VP acknowledges financial support from the European Research Council through the advanced grant No. 694544-OMNES, and from the Deutsche Forschungsgemeinschaft through the DFG projects KL 645/20-1, KL 645/20-2. VP thanks the Department of Physics "E. R. Caianiello" for hospitality and for short visits partial supports (FARB 2018 - 2019) during which the work was completed.

*Data availability statement*: All data that support the findings of this study are included within the article (and any supplementary files).

REFERENCES

[1] Verstraete F., Wolf M. M. and Cirac J. I., *Nat. Phys.*, **5** (2009) 633.
[2] Zanardi P. and Venuti L. C., *Phys. Rev. Lett.*, **113** (2014) 240406.
[3] Albert V. V., Bradlyn B., Fraas M and Jiang L., *Phys. Rev. X*, **6** (2016) 041031.
[4] Touzard S., Grimm A., Leghtas Z. Mundhada S. O., Reinhold P., Axline C., Reagor M., Chou K., Blumoff J., Sliwa K. M., Shankar S., Frunzio L., Schoelkopf R. J., Mirrahimi M. and Devoret M. H., *Phys. Rev. X*, **8** (2018) 021005.
[5] Cole D. C., Wu J. J., Erickson S. D., Hou P.-Y., Wilson A. C., Leibfried D. and Reiter F., *New J. Phys.*, **23** (2021) 073001.
[6] Orioli A. P., Thompson J. K. and Rey A. M., *Phys. Rev. X*, **12** (2022) 011054.
[7] Barontini G., Hohmann L., Haas F. Esteve J. and Reichel J., *Science*, **349** (2015) 1317.
[8] Botzung T., Diehl S. and Müller M., *Phys. Rev. B*, **104** (2021) 184422.
[9] Bardyn C.-E., Baranov M. A., Kraus C. V., Rico E. İmamoğlu A., Zoller P. and Diehl S., *New J. Phys.*, **15** (2013) 085001.
[10] Kollath C., Sheikhan A., Wolff S. and Brennecke F., *Phys. Rev. Lett.*, **116** (2016) 060401.
[11] Barreiro J. T., Mueller M. Schindler P., Nigg D., Monz T., Chwalla M., Hennrich M., Roos C. F., Zoller P. and Blatt R., *Nature*, **470** (2011) 486.
[12] Kraus B., Buechler H. P., Diehl S., Kantian A., Micheli A. and Zoller P., *Phys. Rev. A*, **78** (2008) 042307.
[13] Yamamoto N., *Phys. Rev. A*, **72** (2005) 024104.
[14] Popkov V. and Schütz G. M., *Phys. Rev. E*, **95** (2017) 042128.
[15] Popkov V., Zhang X. and Klümper A., *Phys. Rev. B*, **104** (2021) L081410.
[16] Zhang X., Klümper A. and Popkov V., *Phys. Rev. B*, **103** (2021) 115435.
[17] Zhang X., Klümper A. and Popkov V., *Phys. Rev. B*, **104** (2021) 195409.
[18] Misra B. and Sudarshan E., *J. Math. Phys.*, **18** (1977) 756.
[19] Koshino K. and Shimizu A., *Phys. Rep.*, **412** (2005) 191.
[20] Itano W., Heinzen D., Bollinger J. and Wineland D., *Phys. Rev. A*, **41** (1990) 2295.
[21] Facchi P., Gorini V., Marmo G., Pascazio S. and Sudharshan E., *Phys. Lett. A*, **275** (2000) 12.
[22] Jepsen P. N., Ho W. W., Amato-Grill J., Dimitrova I., Demler E. and Ketterle W., *Phys. Rev. X*, **11** (2021) 041054.
[23] Jepsen P. N., Lee Y. K. E., Lin H., Dimitrova I., Margalit Y., Ho W. W. and Ketterle W., *Nat. Phys.*, **18** (2022) 899 (arXiv:2110.12043 [cond-mat.quant-gas]).
[24] Breuer H. P. and Petruccione F., *The Theory of Open Quantum Systems* (Oxford University Press, Great Clarendon Street) 2002.
[25] Spohn H., *Lett. Math. Phys.*, **2** (1977) 33.

[26] Popkov V., Essink S., Presilla C. and Schuetz G., *Phys. Rev. A*, **98** (2018) 052110.
[27] Popkov V., Essink S., Kollath C. and Presilla C., *Phys. Rev. A*, **102** (2020) 032205.
[28] Popkov V., Presilla C. and Schmidt J., *Phys. Rev. A*, **95** (2017) 052131.
[29] Popkov V., Schmidt J. and Presilla C., *J. Phys. A Math.*, **50** (2017) 435302.
[30] Salerno M. and Popkov V., *Phys. Rev. E*, **87** (2013) 022108.
[31] Popkov V., Prosen T. and zadnik L., *Phys. Rev. Lett.*, **124** (2020) 160403.
[32] Popkov V., Zhang X. and Prosen T., *Phys. Rev. B*, **105** (2022) L220302.
[33] Posske T. and Thorwart M., *Phys. Rev. Lett.*, **122** (2019) 097204.